Rampant introgressive hybridization in *Pogoniulus* tinkerbirds (Piciformes: Lybiidae) despite millions of years of divergence

Emmanuel C Nwankwo[1], Kim G Mortega[2,†], Athanasios Karageorgos[1], Bridget O Ogolowa[1], Gregory Papagregoriou[1], Gregory F Grether[3], Ara Monadjem[4,5], Alexander N G Kirschel[1]

[1]*Department of Biological Sciences, University of Cyprus, PO Box 20537, Nicosia 1678, Cyprus*
[2]*Max Planck Institute for Ornithology, Department of Migration and Immunoecology, Radolfzell, Germany*
[3]*Department of Ecology and Evolutionary Biology, University of California, 621 Charles E. Young Drive South, Los Angeles, CA 90095, USA*
[4]*Department of Biological Sciences, University of Eswatini, Kwaluseni, Swaziland*
[5]*Mammal Research Institute, University of Pretoria, Pretoria, South Africa*
[†]*Current address: Museum für Naturkunde, Leibniz Institute for Evolution and Biodiversity Science, Berlin, Germany*

Abstract

Incomplete reproductive isolation between related species of birds at contact zones is increasingly being documented. Such hybridization typically occurs between sister taxa that diverged in relatively recent times, and hybrids are most often identified based on their intermediate phenotypic characteristics and, increasingly, through genetic admixture analysis. When species have been diverging over relatively longer time scales, prezygotic isolation barriers are expected to evolve, precluding maladaptive interbreeding. Here, we examine the extent of introgressive hybridization in a pair of African barbets, the yellow-fronted tinkerbird (*Pogoniulus chrysoconus extoni*) and the red-fronted tinkerbird (*Pogoniulus pusillus pusillus*), which were not previously known to interbreed, across a contact zone in Southern Africa. Although there were significant differences in the coloration of plumage between the species, we found a pattern of extensive admixture in and around the contact zone. Nonetheless, the two species appear to have diverged > 4 Mya and might not even be sister taxa, suggesting that time of divergence alone might not be sufficient for the evolution of prezygotic reproductive barriers. Significantly more phenotypically red-fronted individuals had a *P. c. extoni* (yellow-fronted) genetic background than vice versa, suggesting possible asymmetry in mate preferences. Sexual selection may thus play a role in breaking down species barriers despite the extent of genetic divergence.

Keywords: asymmetry – barbets – contact zones – convergence – interbreeding – introgression – phylogenetics – plumage coloration – speciation – species interactions.

Introduction

The distributions of many pairs of related species are parapatric, with several factors potentially keeping them from coexisting with each other. Beyond the existence of geographical barriers, such as river valleys and mountains (Wallace, 1876), factors may include adaptation to the environment on either side of an ecological gradient (Price & Kirkpatrick, 2009), where gene flow from a central population optimum swamps adaptation at range boundaries (Kirkpatrick & Barton, 1997; Case *et al.*, 2005), and each species is outcompeted in the range of the other species (Price & Kirkpatrick, 2009). Species boundaries may also be maintained by behavioural interference (reviewed by Grether *et al.*, 2013, 2017), through either competitive or reproductive interference (Weir & Price, 2011), with many examples of hybrid zones where related species

*Corresponding author. E-mail: kirschel@ucy.ac.cy

come into contact [e.g. frogs (Littlejohn & Watson, 1985); deer (Senn *et al.*, 2010); crows (Meise, 1928); buntings (Carling & Brumfield, 2008); woodpeckers (Short, 1965; Johnson & Johnson, 1985), *Ficedula* flycatchers (Tegelström & Gelter, 1990); and wood-warblers (Rohwer *et al.*, 2001)].

Where hybridization is maladaptive because hybrids suffer from reduced viability or sterility, especially in the heterogametic sex (Haldane, 1922), reinforcement may be expected to lead to character displacement in traits important in assortative mating (Dobzhansky, 1951; Coyne & Orr, 2004). Reinforcement may also be expected when hybrids are poorly adapted to ecological conditions, if parental forms are adapted to either side of an ecological gradient (Hatfield & Schluter, 1999), or are phenotypically unattractive to either parental form owing to intermediate appearance or communication signals (Svedin *et al.*, 2008). In other cases, especially where hybrids do not suffer such reduced fitness, genes of parental species may introgress deep into one another's distribution (Joseph *et al.*, 2008; Baldassarre *et al.*, 2014).

Hybrids can often be identified by intermediate phenotypic patterns between parental species (Senn *et al.*, 2010; Delmore *et al.*, 2016; Toews *et al.*, 2016). The extent of introgression in the population might not, however, be clear after F1 hybrids have backcrossed with parental forms and resemble parental species (Senn *et al.*, 2010), and introgression of phenotypic traits extends well into the genomic background of interacting species (Brumfield *et al.*, 2001; Baldassarre *et al.*, 2014).

In birds, a minimum of 16.4% of species have been documented hybridizing with at least one other species in nature (McCarthy, 2006). In songbirds, individuals in contact zones may copy the song of heterospecific males and produce mixed song, which might facilitate hybridization (Qvarnstrom *et al.*, 2006). Hybridization is also widespread, however, in avian families without song learning, such as in ducks (Johnsgard, 1967), quails (Gee, 2003) and woodpeckers (Cicero & Johnson, 1995; Moore, 1995; Wiebe, 2000; Randler, 2002; Fuchs *et al.*, 2013; Michalczuk *et al.*, 2014).

Molecular techniques allow for the identification of hybrids using phylogenetic analyses. Mitochondrial DNA (mtDNA) can show evidence of hybridization when there is a mismatch between the phenotype and mitochondrial genotype, but because it is maternally inherited (Wilson *et al.*, 1985), it would not reveal evidence of the extent of introgression through recombination. This does not undermine its usefulness in identifying maternal species within the F1 hybrids (McDevitt *et al.*, 2009). Nuclear DNA is inherited from both parents and recombines, thus it can aid in identifying hybrids of two different species and their backcrosses (Pfennig *et al.*, 2012), with microsatellite markers used effectively for identification of hybrids (Gay *et al.*, 2009; Väli *et al.*, 2010). A combined set of nuclear and mitochondrial markers, in addition to phenotypic traits, can provide a clear understanding of the extent of introgression of genotypic and phenotypic characters across a contact zone.

We examined interpopulation genetic and phenotypic variation in a pair of African barbets (Lybiidae), across the contact zone of the yellow-fronted tinkerbird *Pogoniulus chrysoconus extoni* and the red-fronted tinkerbird *Pogoniulus pusillus pusillus* (Dumont, 1816), with extensive and conspicuous carotenoid-based yellow and red pigmentation on their forecrown feathers, respectively. The two related species meet in a narrow contact zone from NE South Africa to Eswatini (formerly Swaziland), where a previous study found that songs, which are not learned, appear to converge (Monadjem *et al.*, 1994). Yellow-fronted tinkerbirds close to the contact zone have been described with intermediate, orange-coloured crowns, suggestive of interbreeding (Ross, 1970). We investigated the possibility that the two species hybridize by obtaining samples across the contact zone and genotyping them using microsatellite markers. We estimated the age of divergence of the two species by reconstructing a phylogeny using two mitochondrial markers, and we examined possible convergence of phenotypic traits by taking biometric and spectral reflectance measurements from individuals caught in the field across the region. We hypothesized that if introgressive hybridization occurs, it would be reflected in convergent phenotypic traits and suggest a divergence time of < 3 Mya, in line with expectations for hybridizing species pairs at such latitudes (Weir & Price, 2011).

Material and Methods

Study Species and Site

Pogoniulus chrysoconus (Temminck, 1832) and the closely related *Pogoniulus pusillus* are tinkerbirds found primarily in the savannah region of Africa, although the habitat they occupy varies across each species' range (Short & Horne, 2001). In Southern Africa, *P. c. extoni* occurs in drier savannah woodland and *P. p. pusillus* ranges from woodland to coastal forest. The two species meet in a narrow contact zone, ~20 km wide, primarily in northern Eswatini (Monadjem *et al.*, 1994). We performed fieldwork in South Africa and Eswatini from March 2015 to March 2017 at four allopatric yellow-fronted tinkerbird sites in Mpumalanga, South Africa, four allopatric red-fronted tinkerbird sites in Eswatini and

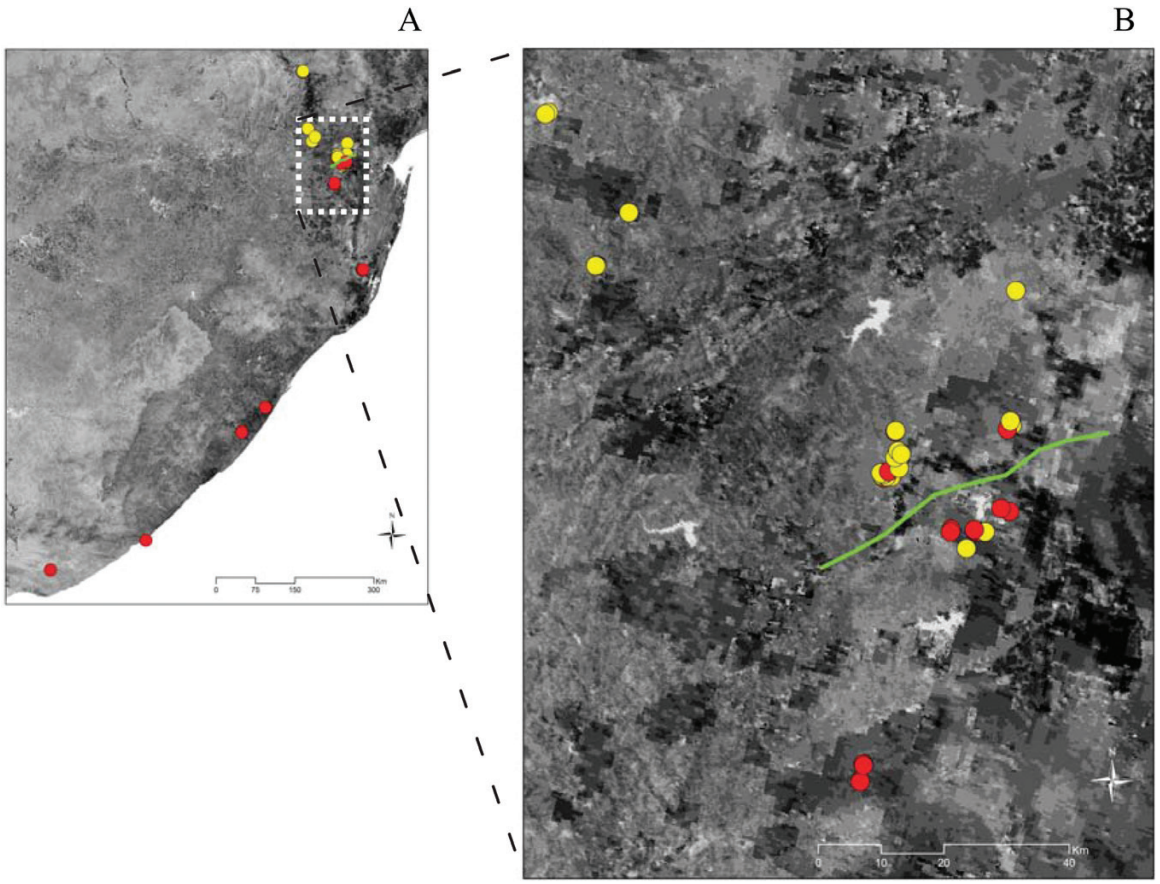

Figure 1. A, distribution of samples of *Pogoniulus chrysoconus extoni* and *Pogoniulus pusillus pusillus* (yellow and red circles, respectively) used in molecular and plumage analyses. The contact zone is illustrated in green, and the background map is an enhanced vegetation index image from the MODIS satellite, with darker shades indicating more densely vegetated areas. B, map illustrating the distribution of samples from populations in sympatry and close by in allopatry (< 100 km). The green contact line is drawn in approximately to divide sympatric sites with a predominance of yellow-fronted and red-fronted phenotypes all shown within a few kilometres of the line.

Kwazulu-Natal, South Africa, and three sympatric sites, two in Eswatini and one in South Africa (Fig. 1).

Morphological Data Collection

Tinkerbirds were captured using targeted mist netting with conspecific playback, and given a metal and colour ring combination. We took biometric measurements from 74 individuals captured in the field: 33 red-fronted and 41 yellow-fronted tinkerbirds. Measurements were taken using digital callipers and included wing chord, tarsus and tail length, culmen length from anterior of the nares, and (exposed) bill length, width and bill depth, and three to five forecrown feather samples were collected for reflectance spectrometry in the laboratory. Geographical coordinates of field sampling locations identified from hand-held Garmin GPS devices were used to obtain the vegetation characteristics of the surveyed locations from Moderate Resolution Imaging Radiometer (MODIS) raster files at 250 m resolution for 2010, from which we extracted vegetation continuous field (VCF) data for field sites in ArcGIS v.10.1 (Environmental Systems Research Institute, 2012, Redlands, CA, USA). Elevation data were obtained from Google Earth (Google, Inc.).

Owing to concerns regarding inter-observer consistency, using measurements from the 39 individuals measured by one of us (A.N.G.K.) from nine populations across the contact zone, we performed a principal components analysis (PCA) with varimax rotation (performed in STATA v.11.2; StataCorp, College Station, TX, USA) to reduce the data for the body dimensions of mass, wing, tarsus and tail to two principal components (PCs) and the four bill dimensions to two further PCs. These PCs were then used to test for variation in morphology resulting from differences between the species, latitude, the

environmental factors (VCF and elevation) and distance to the contact zone using a generalized linear mixed effects model (GLMM) implemented in *lme4* in R v.3.5.1 (Bates *et al.*, 2015), with population assignment included as a random factor. Models were selected based on the lowest Akaike information criterion score corrected for small sample sizes (AICc).

Plumage Coloration and Pattern Analysis

The primary focus of the colour comparison was on the forecrown patch of the two species. It is the most striking difference in plumage between the two species, although some other plumage patterns vary more subtly between the species (Short & Horne, 2001). We measured reflectance spectra (300–700 nm) of feathers on the forecrown using a JAZ spectrometer (Ocean Optics) with a fibre-optic reflectance probe (Ocean Optics R-200) and PX xenon light source. The reflection probe was placed in an RPH-1 reflection probe holder (Ocean Optics), at an angle of 90°, and secured at 2 mm from the aperture of the probe holder. Two measurements were taken per sample, with feathers placed flat onto a black background perpendicular to the observer and facing to the left, and then rotated 180° for the second measurement, with the probe holder placed horizontally onto the feathers, so that the aperture completely covered the feather sample, thus ensuring that ambient light was excluded. Reflectance data for each specimen were obtained after calibration with a white standard (Ocean Optics WS-1) and dark standard (by screwing the lid back onto the fibre-optic connector), and recorded in SPECTRASuite (v.1.0; Ocean Optics).

Specific quantitative variables that were measured from plumage patches within a wavelength range of 300–700 nm included colour distance between individuals from sympatric and allopatric populations of each species (defined based on crown colour), segment classification of the individual plumage patch, and hue differences (Endler *et al.*, 2005; Stoddard & Prum, 2008).

Analysis of plumage colour was performed using R v.3.3.3 (R Core Team, 2017) to implement pavo (an R package for the perceptual analysis, visualization and organization of colour data; Maia *et al.*, 2013). Visual inspection of replicate reflectance spectra was performed, and replicate measurements were averaged and smoothed using the 'procspec' function within pavo before analysis. The colour distances within and between the populations were calculated by using the function 'coldist', which applies the visual models of Vorobyev *et al.* (1998) to calculate colour distances with receptor noise based on relative photoreceptor densities. The function 'segclass' was used to calculate segment classification measures as defined by Endler (1990). A two-dimensional plot of colour points projected from the tetrahedron to its encapsulating sphere to visualize differences in hue was produced using the function 'projplot'. We used the Mollweide projection in the hue projection plot because it preserves area relationships within latitudes without distortion. The avian tetracolourspace visual model was computed using the 'tcs' function to calculate the coordinates and colourimetric variables that represent reflectance spectra in avian tetrahedral colour space: u, s, m and l (the quantum catch data); and x, y and z (cartesian coordinates for the points in tetrahedral colour space). The visual system used was the spectral sensitivity data from the blue tit (*Cyanistes caeruleus*; Hart *et al.*, 2000), and we selected the forest shade illumination model within the avian tetracolourspace model because the study species are canopy dwellers. We estimated colour, following the method described by Endler (1990), by computing three standard descriptors of reflectance spectra: brightness, chroma and hue. Brightness represents the total amount of light reflected by the feather and was calculated as the mean of the summed reflectance from 300 to 700 nm, whereas chroma is a measure of the 'purity' or 'saturation' of a colour. Hue was calculated as the wavelength (in nanometres) corresponding to maximal reflectance (l_{max}), which indicates the principal colour reflected by the feather.

Categorical description analysis of colourimetric variables within the FactoMineR package (Lê *et al.*, 2008) was used to select variables that best described the species according to the plumage patch at $P \leq 0.05$. Subsequently, the selected variables were used in permutational multivariate ANOVA (with the 'vegan' package; Dixon, 2003) using Euclidean distance matrices for partitioning 'distance matrices' among sources of variation, and fitting linear models (on species as factors) to the matrices using a permutation test of 10 000 iterations.

Genetic Sampling and Analysis

Blood samples were obtained from the ulnar superficial vein (wing) of field-caught tinkerbirds, and six further DNA samples from allopatric populations in South Africa were obtained from museums [two tissue samples of *P. c. extoni* (yellow-fronted) from Mpumalanga courtesy of Louisiana State University Museum of Natural Science (LSUMZ), and four blood samples of *P. p. pusillus* (red-fronted) from Eastern Cape, received from the Museum of Vertebrate Zoology (MVZ) at University of California Berkeley]. Additionally, for the phylogeny we included 15 samples of *Pogoniulus chrysoconus chrysoconus* and *Pogoniulus pusillus affinis* from West and East Africa collected during parallel studies (Kirschel *et al.*, 2018),

and further samples of *P. c. extoni* from East Africa collected in the field and one from Malawi courtesy of the Field Museum of Natural History (FMNH).

DNA was extracted using a Qiagen DNeasy blood and tissue kit, following the manufacturer's protocols (Qiagen, Valencia, CA, USA). Polymerase chain reaction (PCR) was performed to amplify DNA of the mitochondrial cytochrome *b* gene, using the primers L14841 (Kocher *et al.*, 1989) and H4a (Harshman, 1994), and ATPase 6/8 genes, using the primers CO2GQL and C03HMH (Eberhard & Bermingham, 2004), on an Applied Biosystems Thermal Cycler (model 2720), with the resulting bands visualized by gel electrophoresis on a 1% agarose gel. The DNA sequences were aligned using Muscle (Edgar, 2004), implemented in MEGA software v.7 (Kumar *et al.*, 2016). We added an outgroup sequence for *Tricholaema diademata* (GenBank: MG230178, MG697232) and performed analyses on combined loci of cytochrome *b* and ATPase 6/8 genes, culminating in an 1859 bp concatenated sequence.

Using the cytochrome *b* sequences, we calculated within POPART: (1) the number of sites that differ among individuals, as an estimate of the number of segregating sites; (2) the number of sites containing at least two states that occur in at least two sequences each, as an estimate of the number of Parsimony-informative sites; (3) Tajima's *D* (Tajima, 1989), which estimates the extent of of selection among the populations; and (4) the molecular variation among populations [analysis of molecular variance (AMOVA); Excoffier *et al.*, 1992]. We assessed genetic relatedness between haplotypes of cytochrome *b* by generating minimum-spanning networks using POPART (Leigh *et al.*, 2015). We then performed a Fisher's exact test in STATA v.11.2 to determine the extent to which haplotypes corresponded to phenotype based on the forecrown colour identified in the field for individuals in sympatry.

Microsatellite Analysis

Fifteen microsatellite loci developed for zebra finch *Taeniopygia guttata*, chicken *Gallus gallus* (Dawson *et al.*, 2010, 2013) and barn owl *Tyto alba* (Klein *et al.*, 2009) were amplified for 81 samples without multiplexes using M13 fluorescent labelling primers. The PCR products were electrophoresed on an ABI 3130xl Genetic Analyser with GeneScan 500 LIZ size standard (Applied Biosystems) and allele sizes determined using GeneMapper (Applied Biosystems).

AMOVA, number of alleles, allelic richness, the observed and expected heterozygosities, and a PCA were performed using the *poppr* (Kamvar *et al.*, 2014), *adegenet* (Jombart, 2008) and *ade4* (Dray & Dufour, 2007) packages in R v.3.4.2 (R Core Team, 2017). Hybridization was tested between species using a Bayesian admixture analysis approach implemented in STRUCTURE v.2.2 (Pritchard *et al.*, 2000) to obtain individual genetic assignment to *P. c. extoni*, *P. p. pusillus* or their hybrids based on the 15 microsatellite loci. We allowed for five independent runs for each simulated value of *K* (*K* = 1–15) populations. STRUCTURE was run using 5 million iterations, with a burn-in of 100 000 iterations. The Evanno method was used to determine the best *K* value (Evanno *et al.*, 2005) in STRUCTURE Harvester v.0.6.1 (Earl & Vonholdt, 2012) while averaging across iterations using the CLUster Matching and Permutation Program (CLUMPP; Jakobsson & Rosenberg, 2007). The output from CLUMPP was visualized using the program DISTRUCT v.1.1 (Rosenberg, 2004).

We screened our microsatellite data to determine populations with fixed alleles and removed uninformative loci from downstream analyses. The 14 sites from which the samples were obtained were grouped into three populations as follows (Fig. 1): *P. p. pusillus* in allopatry comprising six sites (21 samples), *P. c. extoni* in allopatry comprising five sites (15 samples), and sympatry comprising three sites (45 samples).

The strength of our data in discriminating between unique individuals given a random number of loci was determined based on a genotype accumulation curve (Supporting Information, Fig. S1). The overall quality of our multilocus genotype loci (MLG) data was examined, including a search for missing data and rare alleles.

The genotypic diversity indices for each of the populations were estimated: number of MLG observed as an estimate of genotypic richness; number of expected MLG at the smallest sample size ≥ 10 based on rarefaction (eMLG); standard error based on eMLG (SE), Shannon–Wiener index of MLG diversity (Shannon, 1948); Stoddart and Taylor's index of MLG diversity (Stoddart & Taylor, 1988); lambda (Simpson's index; (Simpson, 1949); evenness (E.5; Pielou, 1975); and Nei's unbiased gene diversity (H_{exp}; Nei, 1978).

AMOVA (Excoffier *et al.*, 1992) was implemented using Prevosti's distance (Prevosti *et al.*, 1975), with populations classified for the specified strata field as *P. p. pusillus* (allopatry), *P. c. extoni* (allopatry) and sympatry. Population structure would be evident if most of the variance occurred among rather than within populations. The extent of population differentiation (*D*) ranges from zero for a panmictic population to one for complete differentiation (Meirmans & Hedrick, 2011). The discriminant analysis of principal components (DAPC; Jombart *et al.*, 2010) was used to describe the genetic structure between the allopatry populations of both species and the sympatry population. The number of axes

(n.pca = 50) retained in the PCA step and the number of axes (n.da = 2) retained in the discriminant analysis step were interactively selected as implemented with the 'dapc' function in the *adegenet* R statistical package (Jombart, 2008).

Phylogenetic Analysis

For Bayesian inference (BI) phylogenetic reconstruction based on the combined loci of cytochrome *b* and ATPase 6/8 genes, we ran MrBayes v.3.2.6 (Ronquist *et al.*, 2012), as implemented in Geneious v.11.1.14 (Kearse *et al.*, 2012) with eight Markov chain Monte Carlo (MCMC), which were run for 10^7 generations, with a burn-in of 100 000, sampling every 1000 generations. Convergence from the independent runs and Effective Sample Size (ESS) values were evaluated in Geneious v.11.1.14 (Kearse *et al.*, 2012), with all ESS values > 5000. We determined the best partitioning schemes and corresponding nucleotide substitution models for each codon position of the genes using PartitionFinder 2 (Lanfear *et al.*, 2016). The corrected AICc and the 'greedy' algorithm with branch lengths estimated as unlinked were used to search for the best-fitting scheme. Phylogenetic analyses were conducted using Bayesian phylogenetic reconstruction based on the six data partitions as follows (for ATPase and cytochrome *b*, respectively: first codon position, both GTR+G; second codon position, both GTR+I+G; and third codon position GTR+G and GTR+I+G). We ran maximum likelihood analysis using RAxML v.8.2.11 (Stamatakis, 2014), as implemented in Geneious, on the six data partitions with 1000 rapid bootstrap inferences and thereafter a thorough ML search, using the GAMMA model of rate heterogeneity and the GTR substitution model.

Divergence dates were estimated in BEAST 2 (Prlic *et al.*, 2014), with five sequences added from GenBank for calibration based on the ages of divergence of Hawaiian honeycreepers described by Lerner *et al.* (2011), in addition to one Picidae sequence for the outgroup. We used a strict clock model and a gamma prior for birth rate and clock rate. The MCMC analysis was run for 25 million generations, sampling every 2500 generations. The final tree was produced from the generated trees by compiling a maximum posteriori tree using a burn-in of 10% in TreeAnnotator v.2 (Rambaut & Drummond, 2014). Convergence from the independent runs and ESS values were evaluated in Tracer v.1.6 (Rambaut *et al.*, 2014).

Genetic and Phenotypic Cline analysis

We conducted geographical cline analysis along the transect from the northernmost yellow-fronted tinkerbird site at Blyde River Canyon (–168 km) to the southernmost red-fronted tinkerbird site at Table Farm (925 km), with 0 km marking the estimated contact line (Fig. 1), using the Metropolis–Hastings MCMC algorithm implemented within the package HZAR (Derryberry *et al.*, 2014) to fit genetic and phenotypic clines and estimate the cline centre and width for each trait. The cline analyses were fitted to different combinations of the exponential decay curve parameters δ and *s* using models described by Derryberry *et al.* (2014) as follows: model I, p_{min}/p_{max} (the minimum and maximum estimated frequencies at each end of the cline) set to observed values with no exponential decay curves (or tails) fitted; model II, p_{min}/p_{max} estimated with no tails fitted; and model III, p_{min}/p_{max} estimated and both tails fitted, for each of the mitochondrial DNA haplotype, STRUCTURE Q values from the combined microsatellite dataset, the plumage coloration measures of brightness, hue and chroma, and wing chord length. Model selection was based on the AICc, and the model with the lowest AICc was selected as the best-fitting model. We compared the support limits of two log-likelihood units from the cline centres to determine the concordance of genetic and phenotypic clines.

Results

Biometrics

Of the 39 individuals ringed and included in the morphological analysis, 19 were identified in the field as yellow-fronted and 20 as red-fronted tinkerbirds based on the colour of the forecrown. The two PCs retained for each of the PCAs for body size and bill size explained 75 and 76% of the variation, respectively (see Supporting Information, Tables S1 and S2). For body size, PC1 was positively associated with mass, tarsus and tail length, and PC2 was positively associated with wing length and negatively with tarsus length (Supporting Information, Table S1). For bill size, PC1 was positively associated with two measures of bill length and bill depth, and PC2 was positively associated with bill width (Supporting Information, Table S2). Plots of the PCs suggest that red-fronted tinkerbirds in allopatry are larger overall (PC1) and that yellow-fronted tinkerbirds have longer wings (PC2), whereas there is no obvious pattern distinguishing the species in bill size (Fig. 2). But a number of factors could explain these patterns, and the GLMM found that variation in body size (PC1) was best explained by distance to contact zone and population (distance, $t = 9.105$, $P < 0.00001$; population (intercept), $t = -5.714$, $P < 0.001$; Supporting Information, Table S3), with larger individuals further from the contact zone, and in PC2 by species and population (species, $t = -2.779$, $P < 0.001$; population, $t = 2.232$, $P = 0.026$; Supporting Information, Table S4), indicating that yellow-fronted tinkerbirds have longer

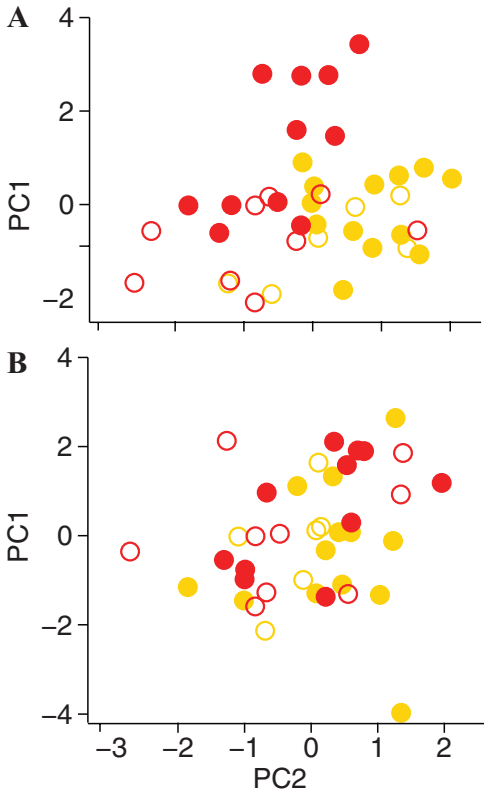

Figure 2. There is much overlap in morphology between the two species. A, in body size, distance to contact zone illustrates the separation of allopatric (filled circles) red-fronted tinkerbirds (red circles) from allopatric yellow-fronted tinkerbirds (amber circles) in principal component (PC)1 (representing mass, tarsus and tail length) and PC2 (representing wing length), with overlap among sympatric individuals (open circles). B, in bill shape, there is substantial overlap in both sympatric and allopatric populations.

wings than red-fronted tinkerbirds. The GLMM also found that species explained some variation in bill size (PC1, t = 2.148, P = 0.032; Supporting Information, Table S5), with red-fronted tinkerbirds having longer, deeper bills than yellow-fronted tinkerbirds, along with elevation and population for PC2 (elevation, t = 2.374, P = 0.018; population, t = –2.06; P = 0.039; Supporting Information, Table S6), suggesting that bills were wider at higher elevations. We found no effect of tree cover on morphology (Supporting Information, Tables S3–S6).

Plumage Coloration

Colour distance and segment classification of forecrown colour

Crown colour was distinct between yellow- and red-fronted tinkerbirds across all measures of plumage coloration. Specifically, there were significant differences in chromatic distance among populations of the two species in sympatry and allopatry ($F_{9,1643}$ = 48.519, R^2 = 0.2099, P = 0.0001; Supporting Information, Fig. S1), with allopatric populations of the two species being more different than sympatric pairs. Scoring colour points between the short- and long-wavelength spectrum based on segment classification measures (Endler, 1990) revealed that the colour points fall within the red–orange–yellow regions of the spectrum. There were significant differences among the four groups of yellow-fronted and red-fronted tinkerbirds in sympatry and allopatry within the colour spectrum ($F_{3,54}$ = 17.541, R^2 = 0.49354, P = 0.0001; Supporting Information, Fig. S2), and the variation in colour within each group (0.1610) was lower than between each group (0.2542) (Supporting Information, Fig. S1).

Hue, brightness and chroma

Visualizing differences in hue based on a plot of colour points projected from the tetrahedron to its encapsulating sphere showed that the hue of crown plumage patch is between green and red longitudes and specifically in the red–yellow region (Supporting Information, Fig. S3). ANOVA based on Euclidean distances revealed significant differences in hue, brightness and chroma of the crown plumage patch among the populations of the two species ($F_{3,54}$ = 13.924, R^2 = 0.44, P = 0.0001; Fig. 3A–C). Specifically, the highest hue score was found in allopatric *P. c. extoni* and sympatric *P. c. extoni*, followed by sympatric *P. p. pusillus*, and lowest in allopatric *P. p. pusillus* ($F_{3,54}$ = 52.85, R^2 = 0.7318, P < 0.0001). Chroma, in contrast, was highest in allopatric *P. p. pusillus*, followed by sympatric *P. p. pusillus*, and lowest in allopatric *P. c. extoni* ($F_{3,54}$ = 7.436, R^2 = 0.253, P = 0.0002). There were also significant differences in the mean brightness of the crown patch among the populations ($F_{3,54}$ = 8.126, R^2 = 0.2728, P = 0.0001). Crown brightness was highest in allopatric and sympatric *P. c. extoni*, lower and similar in allopatric and sympatric *P. p. pusillus*.

Tetracolour plot and model

Based on the tetracolourspace variables (s, l and m) and using multivariate permutational ANOVA, we found significant differences in the crown of the species across the populations ($F_{3,54}$ = 55.32, R^2 = 74, P < 0.0001; Supporting Information, Fig. S3). Specifically, allopatric *P. p. pusillus* showed highest reflectance within the long wavelength but least in short and medium wavelengths. The reflectance of the sympatric populations for both species were similar within the short wavelength

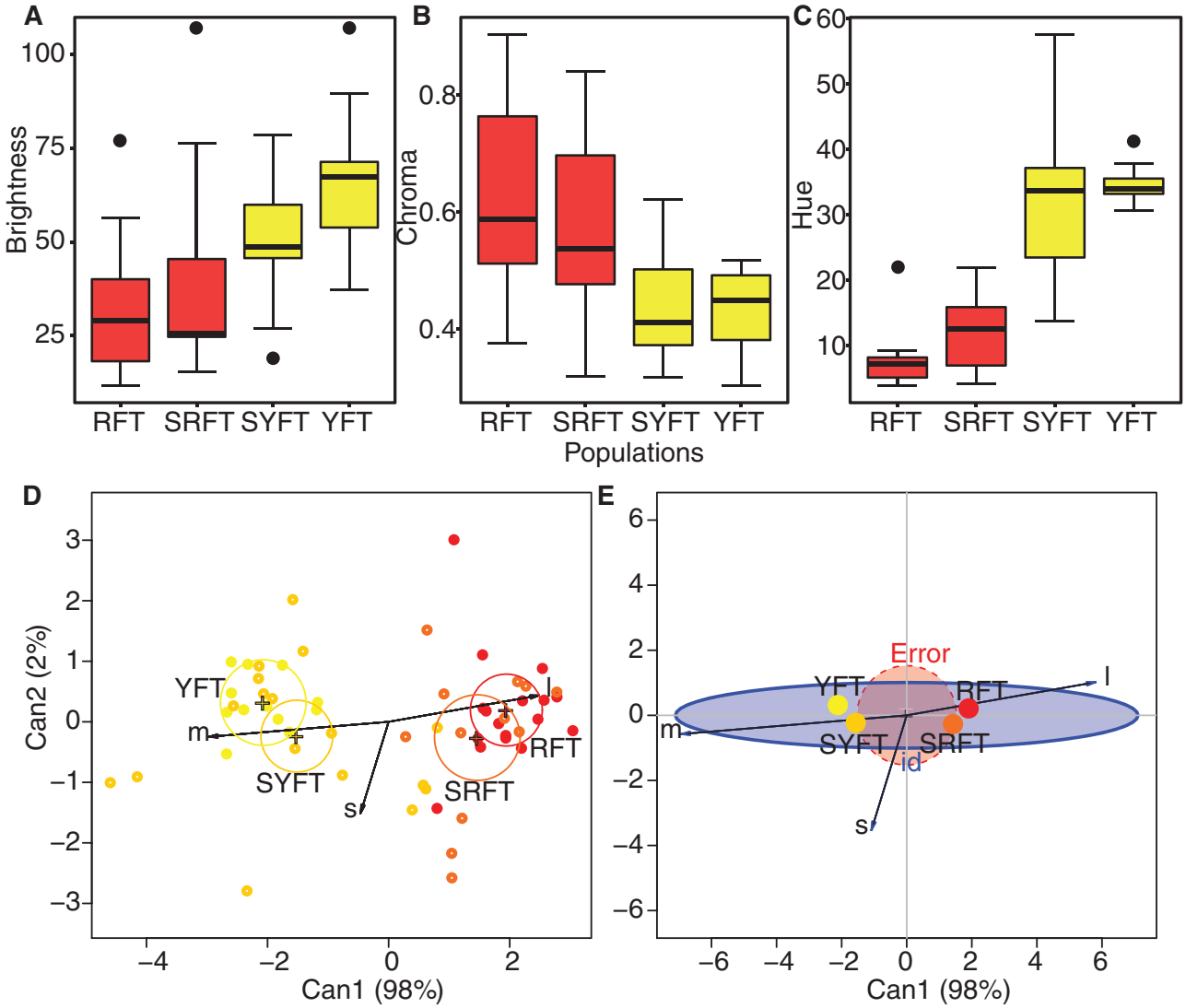

Figure 3. A–C, boxplots illustrating forecrown brightness (A), chroma (B) and hue (C) in allopatric and sympatric populations of the two species (RFT, allopatric *Pogoniulus pusillus*; SRFT, sympatric *P. pusillus*; YFT, allopatric *Pogoniulus chrysoconus*; and SYFT, sympatric *P. chrysoconus*). There is evidence of individuals with intermediate phenotypes (based on the interquartile range) in sympatry, in brightness in SYFT, in chroma in SRFT, and in hue in both. D, E, canonical discriminant analysis plot for individuals (D) and population means (E), based on the colour points estimated from the tetracolourspace model for the populations: RFT (red dots), SRFT (orange), YFT (yellow) and SYFT (amber). Arrows represent position in the short- (*s*), medium- (*m*) and long-wave (*l*) spectrum.

but not in the long and medium wavelengths. Allopatric *P. c. extoni* showed the highest reflectance within the medium wavelength but least in the short wavelength. Canonical discriminant analysis on the tetracolourspace variables showed that sympatric and allopatric populations of the respective species were closer to each other, but that individuals within the error region of classification were mainly from the sympatric population for both species (Fig. 3D, E).

Microsatellite analysis

Of the 15 microsatellite loci amplified, ten were variable and without null alleles and were subsequently used for analysis. Eight microsatellite loci were found to be in Hardy–Weinberg equilibrium, and 81 alleles were recovered. A permutation test on the optimal number of markers required to distinguish sufficiently between individuals plateaued at six loci (Supporting Information, Fig. S4). Heterozygosity with population structure (H_{ST} and G_{ST}) was greater at three loci (CAM13, CAM17

and TG02088) relative to other loci, and heterozygosity without population structure (H_T and $G_{prime-ST}$) was greater at six loci (CAM13, CAM17, TG02088, Bb111TG, CAM18 and TG13009; Supporting Information, Fig. S4; Table S7) compared with other loci. Population differentiation (D) was highest at loci CAM13 and TG13009 (Supporting Information, Fig. S4; Table S7).

Based on pairwise genetic differentiation analysis (G_{ST}), we found that *P. c. extoni* (YFT) in allopatry were less differentiated from the sympatric population (0.112) than was *P. p. pusillus* (RFT) in allopatry (0.3156). The highest levels of genetic differentiation were, as expected, observed between allopatric *P. c. extoni* and allopatric *P. p. pusillus* (0.5152). Genotype richness was highest in sympatry, followed by *P. p. pusillus* in allopatry, and was least in *P. c. extoni* in allopatry based on the Shannon–Wiener index of MLG diversity (H), Stoddart and Taylor's index of MLG diversity (G), Nei's unbiased gene diversity (H_{exp}) and the number of multilocus genotypes (MLG) observed. The recovered genotypes were evenly distributed within the population based on Pielou's index (E.5), and the expected MLG (eMLG) was the same among the two allopatric populations and those in sympatry (Supporting Information, Table S8).

AMOVA revealed significant variation in genotype in terms of distance from the contact zone ($\sigma^2 = 3.278$, $P < 0.0001$) and at the population level ($\sigma^2 = 4.097$, $P < 0.0001$). The coefficient of molecular variation was higher when comparing between allopatric populations and sympatry ($a = 23.888$) than among sampling sites ($a = 4.7094$). The PCA showed that allopatric *P. p. pusillus* were substantially more differentiated from the sympatric population than the latter was from allopatric *P. c. extoni* (Supporting Information, Fig. S5).

Although we do not assign a threshold for pure individuals of each species, STRUCTURE analysis found that 12/15 individuals of the yellow-fronted tinkerbird in allopatry (> 20 km from the contact line) had Q > 0.9, with 2/15 having 0.8 < Q < 0.9 and only 1/15 having 0.2 < Q < 0.8, whereas 12/21 individuals of the red-fronted tinkerbird in allopatry had Q > 0.9, 4/21 had 0.8 < Q < 0.9 and 5/21 had 0.2 < Q < 0.8. Thus, more phenotypically red-fronted individuals (eight) grouped genetically with *P. c. extoni* than phenotypically yellow-fronted (one) grouped genetically with *P. p. pusillus*, based on microsatellite markers (Fig. 4; Supporting Information, Fig. S6) and mitochondrial (cytochrome *b*) haplotypes (Supporting Information, Fig. S7).

Phylogentic reconstruction

We sequenced 1033 bp of cytochrome *b* from 81 individuals, which were used to prepare the RAxML tree (Supporting Information, Fig. S7). In addition, we used 1027 bp cytochrome *b* (the 6 bp difference

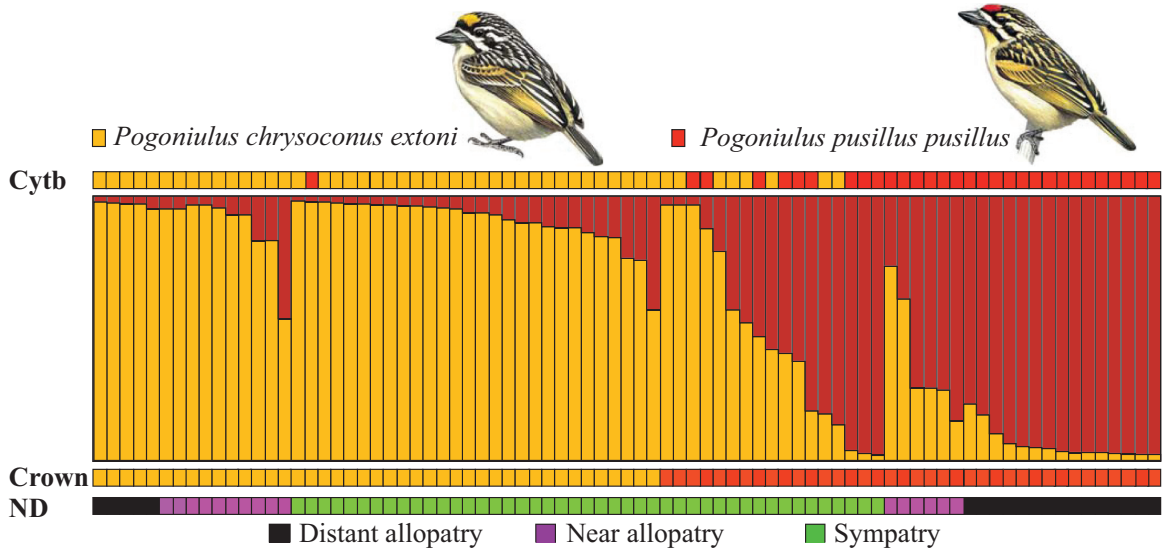

Figure 4. STRUCTURE analysis illustration using the microsatellite data set ($N = 81$ alleles), with *Pogoniulus chrysoconus extoni* genotypes represented in yellow and *Pogoniulus pusillus pusillus* in red. Banners above and below the plot represent the species as identified by mitochondrial DNA haplotypes and phenotypically in the field, respectively. Individuals are arranged from distant allopatric populations of phenotypically yellow-fronted tinkerbirds on the left, along the transect through sympatry towards distant allopatric populations of phenotypically red-fronted tinkerbirds on the right. Tinkerbird illustrations courtesy of del Hoyo *et al.* (2019).

occurred because two codons were missing from the beginning of sequences from individuals from elsewhere in Africa) and 832 bp ATPase sequences for 31 individuals in Bayesian analysis and divergence time estimation.

Bayesian analysis of the concatenated 1859 bp mitochondrial sequence (Fig. 5) revealed that *P. chrysoconus* is paraphyletic with respect to *P. pusillus*, which is monophyletic. The *P. c. extoni* group is basal to *P. c. chrysoconus* and *P. pusillus*. Divergence of the subspecies is highly supported based on their maximal Bayesian posterior probability values. The calibrated Bayesian phylogenetic tree found that *P. c. extoni* has been diverging from *P. c. chrysoconus* and *P. p. pusillus* for 4.41 Myr, *P. c. chrysoconus* from *P. p. pusillus* for 3.28 Myr, and *P. p. pusillus* from *P. p. affinis* for 2.01 Myr (Fig. 5). Uncorrected pairwise sequence divergence between *P. p. pusillus* and *P. c. extoni* was estimated at 8.4%. We recovered 27 segregating sites, nucleotide diversity of $\pi = 0.0245$ and 25 informative sites. Our test for selection among the populations provided evidence of selective pressure, with a significant Tajima's *D* statistic ($D = 2.9347$, $P = 0.0021$). AMOVA based on mtDNA showed higher variation among populations ($\sigma^2 = 664.568$, percentage variation = 52.88) than within populations ($\sigma^2 = 592.082$, percentage variation = 47.11). The minimum spanning network reveals the presence of haplotypes of both species at populations within the contact zone, with the number of individuals with *P. c. extoni* haplotypes within the predominantly red-fronted Tshaneni (Eswatini) population reflecting the extent of introgressive hybridization (Fig. 6). A Fisher's exact test comparing haplotypes with forecrown colour from individuals in sympatry found that there were significantly more red-forecrowned individuals with *P. c. extoni* haplotypes (8/17) and fewer yellow forecrowned individuals with *P. p. pusillus* haplotypes (1/28) than expected by chance ($P = 0.0002$, Fig. 4; Supporting Information, Fig. S7) See Supporting Information, Table S9 for sample details and GenBank accession numbers.

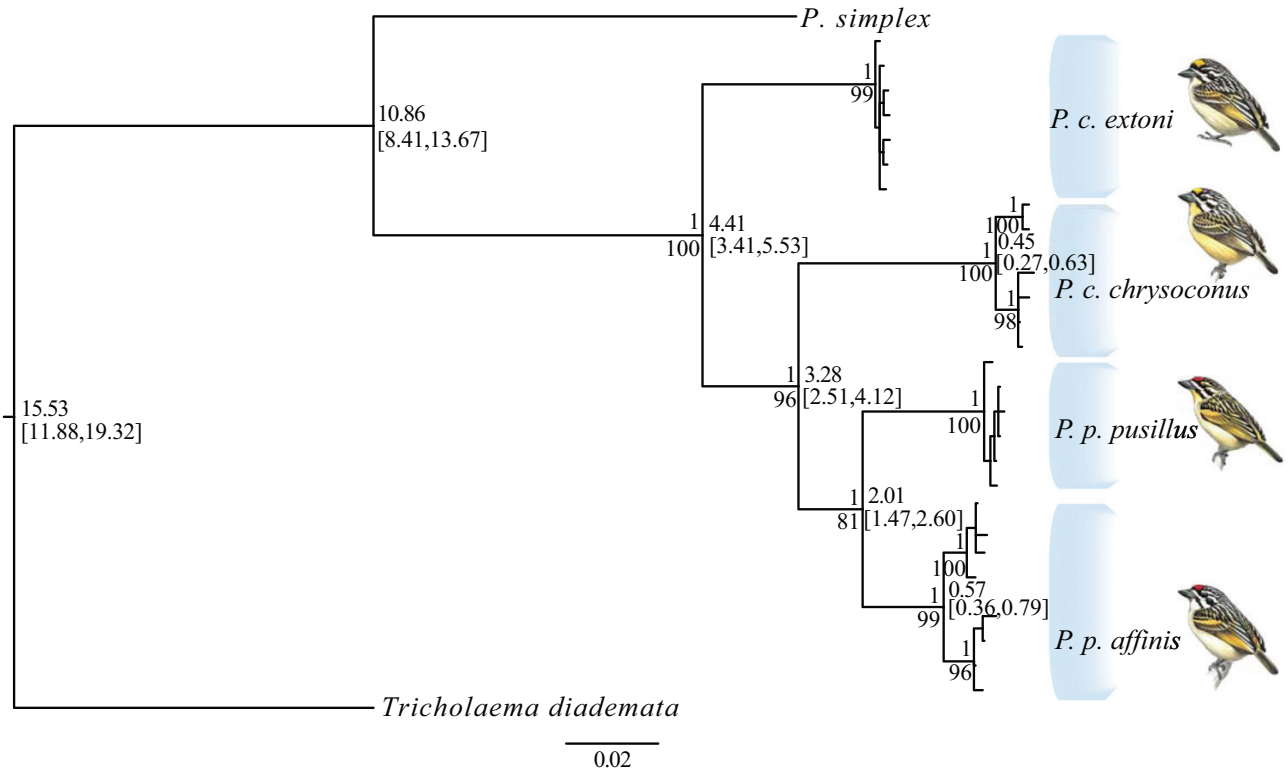

Figure 5. Calibrated phylogenetic tree of *Pogoniulus pusillus* and *Pogoniulus chrysoconus* based on the Bayesian inference consensus and maximum likelihood (ML) trees of cytochrome *b* and ATPase. Leftward of nodes are the posterior probabilities values indicated above and ML bootstrap values below, with node ages (above) and age high posterior density (below) on the right side of the node, estimated using BEAST 2. *Pogoniulus chrysoconus* is paraphyletic, with *Pogoniulus chrysoconus extoni* basal, having diverged > 4 Mya from the clade that includes *P. c. chrysoconus* sister to the *P. pusillus* clade. Tinkerbird illustrations courtesy of del Hoyo *et al.* (2019).

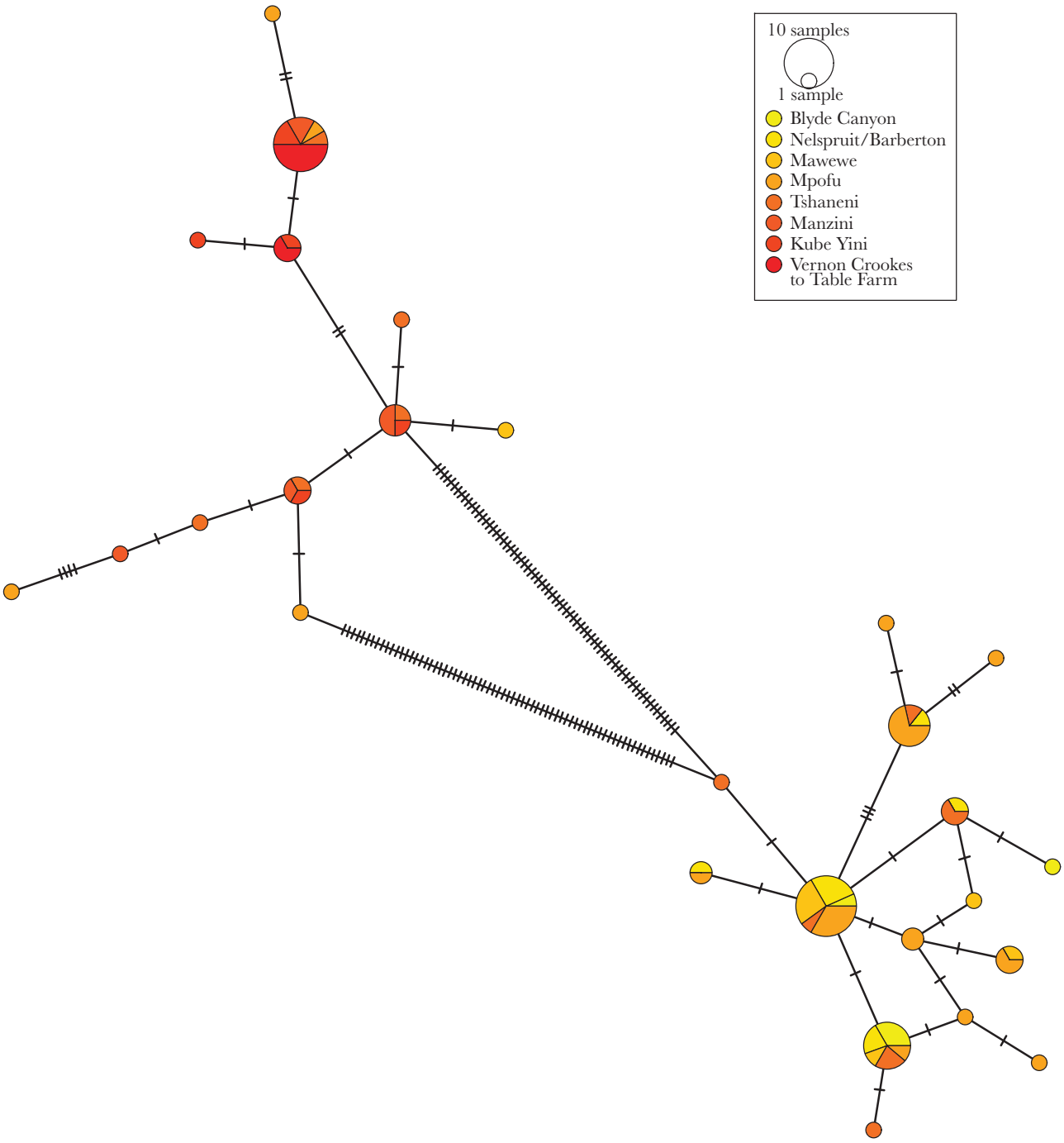

Figure 6. Cytochrome *b* haplotype network by population, coloured using a gradient along the transect from *Pogoniulus chrysoconus extoni* in allopatry (in yellow) to *Pogoniulus pusillus pusillus* in allopatry (in red). Here, adjacent populations within 10 km of each other are merged, as are the four allopatric *P. p. pusillus* populations > 400 km from the contact zone. More phenotypically red-fronted tinkerbirds were found with *P. c. extoni* haplotypes than yellow-fronted tinkerbirds found with *P. p. pusillus* haplotypes.

Genetic and phenotypic cline analysis

Cline widths for hue and chroma (17.1 and 1.1 km, respectively) show a sharper transition than the cline width for STRUCTURE Q score (60.8 km; Fig. 7), suggesting much introgression into the genomes of parental (phenotypic) species (although the two log-likelihood unit support limits of the two coloration clines slightly overlapped with those of the STRUCTURE Q

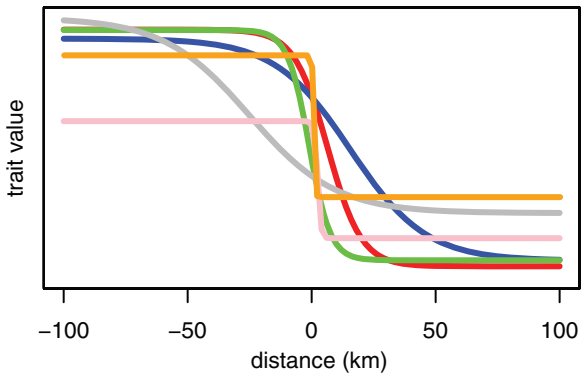

Figure 7. The maximum-likelihood clines for STRUCTURE Q values from microsatellites (blue), cytochrome *b* (red), hue (green), chroma (orange), brightness (grey) and wing length (pink), across the contact zone. Plumage coloration clines are offset from molecular and morphological clines. Negative distances represent individuals on the *Pogoniulus chrysoconus extoni* (north) side and positive distances those on the *Pogoniulus pusillus pusillus* (south) side of the cline. The distances were measured in kilometres for each population perpendicular to the contact zone at 0 km.

cline; Supporting Information, Table S10). The cline width for brightness was much wider (69.3 km), but its cline centre (−25.1 km) was offset significantly to the north, into the *P. c. extoni* genomic region, as was hue (−1.1 km), compared with the STRUCTURE Q cline centre (15.6 km), with chroma (0.1 km) and wing (2.4 km) also to the north of the genetic cline centre, albeit not significantly different from it. The mtDNA cline centre was intermediate between these, at 6.5 km (Fig. 7; Supporting Information, Table S10). The four phenotypic clines were all thus offset to the north of the two genetic clines, with none to the south, suggesting asymmetric introgression.

Discussion

Our analyses reveal rampant introgressive hybridization in the contact zone between *P. p. pusillus* and *P. c. extoni*, with almost all individuals in the contact zone showing some evidence of introgression, as do some individuals in near allopatry, with the cline in microsatellites > 60 km wide. This level of introgressive hybridization is in spite of the extent of divergence between the two species in mtDNA (8.4% pairwise sequence divergence) and significant differences in forecrown plumage coloration. There is also substantial overlap in morphological characters at the contact zone, which based on our analyses, is most probably explained by introgressive hybridization, with allopatric populations of both species differing in morphology from sympatric populations.

Introgressive hybridization appeared primarily asymmetric, with more phenotypically red-fronted individuals being identified as *P. c. extoni* based on mtDNA haplotypes and nuclear markers within the contact zone than vice versa, suggesting the predominant occurrence of backcrossing into the *P. c. extoni* lineage. The PCA on the microsatellite data showed a clear separation of allopatric populations of *P. c. extoni* and *P. p. pusillus* into two distinct clusters and an intermediate position for sympatric populations (Supporting Information, Fig. S5). This indicates that gene flow between the two subspecies has resulted in a high degree of allele sharing between individuals in sympatry. The pattern of asymmetric introgression of *P. p. pusillus* genes and forecrown colour into the genetic background of *P. c. extoni* based on the analyses presented here might have resulted from a sexual preference for red-fronted males by both yellow-fronted and red-fronted females, although we cannot rule out the possibility that hybrid individuals with *P. p. pusillus* mothers suffer from reduced fitness, nor the possibility of genetic dominance of red over yellow alleles (Butlin & Neems, 1994). STRUCTURE clustering analysis further supports the presense of hybridization between the species, with the highest likelihood values supporting $K = 2$ populations, representing the allopatric populations of the two species, with individuals from the contact zone showing much evidence of admixture.

In most studies on introgression at contact zones, there is clear evidence of mixing of plumage traits that make hybrid identification straightforward (Cicero & Johnson, 1995; Poelstra *et al.*, 2014; Toews *et al.*, 2016; but see Baldassarre *et al.*, 2014; McLean *et al.*, 2017), and hybridization occurs among some species with comparatively little divergence in mtDNA (e.g. (Lovette *et al.*, 1999; Poelstra *et al.*, 2014; Toews *et al.*, 2016; Oatley *et al.*, 2017). Here, hybridization occurs at very high levels despite > 4 Myr of divergence, similar to levels reported only in *Willisornis* antbirds (Weir *et al.*, 2015) and *Passerina* buntings (Klicka *et al.*, 2001; Carling *et al.*, 2010) among commonly hybridizing species. In the buntings, strong sexual selection appears to have driven dichromatism and elaborate plumage coloration in *Passerina amoena* and *Passerina cyanea*, but asymmetric hybridization at the contact zone leads to extensive introgression from one species into the genome of the other, with clearly identifiable hybrids that have intermediate plumage (Carling & Brumfield, 2008). In the present study, with sexes alike, the primary plumage character used to distinguish between the species, forecrown colour, remained distinct between yellow-fronted and red-fronted tinkerbirds, in spite of some evidence of smaller differences in sympatry (see also Ross, 1970),

but with no overlap at the contact zone. However, other plumage characters, such as throat, rump and belly colour, represented by different shades of yellow, could better reflect levels of introgression, and future work might investigate the extent to which some plumage patterns introgress between species while others remain distinct.

Plumage coloration plays a significant role in mate choice and may explain asymmetric patterns of hybridization in *Manacus* manakins (Brumfield *et al.*, 2001), *Passerina* buntings (Carling & Brumfield, 2008) and *Malurus* fairy-wrens (Baldassarre *et al.*, 2014). In our study, there is evidence for asymmetric introgression of red forecrown plumage into the *P. c. extoni* genetic background. Such a pattern could result from a preference for red plumage coloration in males by *P. c. extoni* females, and ongoing work is focusing on identifying genes responsible for red and yellow plumage across the hybrid zone (A. N. G. Kirschel, unpublished data). Alternatively, forecrown plumage coloration could play a role in intrasexual dynamics (e.g. Pryke & Griffith, 2006), with red-forecrowned males potentially dominant over yellow.

Another phenotypic trait mediating interspecific interactions in birds is song (Orians & Willson, 1964; Kirschel *et al.*, 2009b; Tobias & Seddon, 2009; Grant & Grant, 2010; Laiolo, 2012). Studies on passerines have found instances of song mixing both facilitating hybridization (Qvarnstrom *et al.*, 2006) and maintaining range boundaries between ecological competitors that hybridize (McEntee *et al.*, 2016), but song has been shown to vary along ecological gradients in Africa (Slabbekoorn & Smith, 2002; Kirschel *et al.*, 2009a, 2011; Smith *et al.*, 2013), suggesting that there is selective pressure for songs to converge where populations of different species meet. In contrast, previous work on forest tinkerbirds found that songs diverge when related species coexist, reducing costly aggressive interactions (Kirschel *et al.*, 2009b), and that songs can diverge rapidly between populations of the same species, by an order of magnitude faster than between the pair of species studied here (Nwankwo *et al.*, 2018). Yet, a previous study on song in yellow-fronted and red-fronted tinkerbirds found that their songs were more similar in sympatry in Eswatini than in allopatry (Monadjem *et al.*, 1994), implying that song differences may be insufficient to maintain the species boundary and that song characters may introgress among the species. Further studies on the importance of song in species recognition between the two species are ongoing (A. N. G. Kirschel, unpublished data), but the present study suggests that if differences in song are insufficient to maintain positive assortative mating, strong sexual selection for a heterospecific trait, in this case red forecrown plumage, may break down the species boundary and result in asymmetric introgression.

Conclusion

Our findings suggest that in spite of evidence for > 4 Myr of divergence, which resulted in distinct differences in plumage, these two taxa hybridize extensively despite not even being sister taxa according to our phylogenetic analyses, notwithstanding the possibility that the mitochondrial gene tree is discordant with the species tree. Nevertheless, levels of divergence among other subspecies of yellow-fronted and red-fronted tinkerbirds are similarly high, and it remains to be seen what, if any, character might mediate reproductive isolation in other contact zones of the two species elsewhere and what we can then infer from the role of phenotypic characters and genetic divergence in mediating reproductive isolation.

Acknowledgements

We thank P. Mabuza, M. Mamba, D. Nobantu and S. Bulunga for assistance in the field, C. Downs, D. Ehlers Smith, M. Motsa, Z. Ndwandwe, M. and S. McGinn, J. and R. Harding and A. Howland for assistance with logistics, and the following museums (and their staff) for providing tissue loans: LSUMZ (F. Sheldon and D. Dittmann), FMNH (D. Willard and J. Bates) and MVZ (J. Fuchs and R. Bowie). We thank the Kingdom of Eswatini's Big Game and Parks (K. Wright), Mpumalanga Tourism and Parks Agency (N. Shaik) and Ezemvelo KZN Wildlife (B. Coverdale) for assistance with research permits, and SAFRING for ringing permits. We wish to thank C. Deltas, D. Hadjipanagi and C. Koutsofti of the Molecular Medicine Research Center at the University of Cyprus, who offered research infrastructure and expertise for completing this work, and we thank M. Moysi and A. Efstathiou for DNA extractions and PCR, and A. Stylianou for plumage reflectance measurements. We thank two anonymous reviewers for their comments that helped to improve the manuscript. We are especially grateful for the funds provided for the study from a Marie Curie International Reintegration Grant (A.N.G.K.) and the A. P. Leventis Ornithological Research Institute (E.C.N. and B.O.O.).

References

Baldassarre DT, **White TA**, **Karubian J**, **Webster MS. 2014.** Genomic and morphological analysis of a semipermeable avian hybrid zone suggests asymmetrical introgression of a sexual signal. *Evolution* **68:** 2644–2657.

Bates D, **Mächler M**, **Bolker B**, **Walker S. 2015.** Fitting linear mixed-effects models using lme4. *Journal of Statistical Software* **67:** 1–48.

Brumfield RT, **Jernigan RW**, **McDonald DB**, **Braun MJ. 2001.** Evolutionary implications of divergent clines in an avian (*Manacus*: Aves) hybrid zone. *Evolution* **55:** 2070–2087.

Butlin RK, **Neems RM. 1994.** Hybrid zones and sexual selection. *Science* **265:** 122.

Carling MD, **Brumfield RT. 2008.** Haldane's rule in an avian system: using cline theory and divergence population genetics to test for differential introgression of mitochondrial, autosomal, and sex-linked loci across the *Passerina* bunting hybrid zone. *Evolution* **62:** 2600–2615.

Carling MD, **Lovette IJ**, **Brumfield RT. 2010.** Historical divergence and gene flow: coalescent analyses of mitochondrial, autosomal and sex-linked loci in *Passerina* buntings. *Evolution* **64:** 1762–1772.

Case TJ, **Holt RD**, **McPeek MA**, **Keitt TH. 2005.** The community context of species' borders: ecological and evolutionary perspectives. *Oikos* **108:** 28–46.

Cicero C, **Johnson NK. 1995.** Speciation in sapsuckers (*Sphyrapicus*): III. Mitochondrial-DNA sequence divergence at the cytochrome-*b* locus. *The Auk* **112:** 547–563.

Coyne JA, **Orr HA. 2004.** *Speciation*. Sunderland: Sinauer Associates.

Dawson DA, **Ball AD**, **Spurgin LG**, **Martín-Gálvez D**, **Stewart IRK**, **Horsburgh GJ**, **Potter J**, **Molina-Morales M**, **Bicknell AWJ**, **Preston SAJ**, **Ekblom R**, **Slate J**, **Burke T. 2013.** High-utility conserved avian microsatellite markers enable parentage and population studies across a wide range of species. *BMC Genomics* **14:** 176.

Dawson DA, **Horsburgh GJ**, **Küpper C**, **Stewart IRK**, **Ball AD**, **Durrant KL**, **Hansson B**, **Bacon I**, **Bird S**, **Klein Á**, **Krupa AP**, **Lee JW**, **Martín-Gálvez D**, **Simeoni M**, **Smith G**, **Spurgin LG**, **Burke T. 2010.** New methods to identify conserved microsatellite loci and develop primer sets of high cross-species utility – as demonstrated for birds. *Molecular Ecology Resources* **10:** 475–494.

del Hoyo J, **Elliott A**, **Sargatal J**, **Christie DA**, **Kirwan G. 2019.** *Handbook of the Birds of the World Alive*. Barcelona: Lynx Edicions. Available at http://www.hbw.com/ (accessed 8 February 2019).

Delmore KE, **Toews DPL**, **Germain RR**, **Owens GL**, **Irwin DE. 2016.** The genetics of seasonal migration and plumage color. *Current Biology* **26:** 2167–2173.

Derryberry EP, **Derryberry GE**, **Maley JM**, **Brumfield RT. 2014.** HZAR: hybrid zone analysis using an R software package. *Molecular Ecology Resources* **14:** 652–663.

Dixon P. 2003. VEGAN, a package of R functions for community ecology. *Journal of Vegetation Science* **14:** 927–930.

Dobzhansky T. 1951. *Genetics and the origin of species*. New York, London: Columbia University Press.

Dray S, **Dufour A-B. 2007.** The ade4 package: implementing the duality diagram for ecologists. *Journal of Statistical Software* **22:** 1–20.

Earl DA, **Vonholdt BM. 2012.** STRUCTURE HARVESTER: a website and program for visualizing STRUCTURE output and implementing the Evanno method. *Conservation Genetics Resources* **4:** 359–361.

Eberhard JR, **Bermingham E. 2004.** Phylogeny and biogeography of the *Amazona ochrocephala* (Aves: Psittacidae) complex. *The Auk* **121:** 318–332.

Edgar RC. 2004. MUSCLE: a multiple sequence alignment method with reduced time and space complexity. *BMC Bioinformatics* **5:** 113.

Endler JA. 1990. On the measurement and classification of colour in studies of animal colour patterns. *Biological Journal of the Linnean Society* **41:** 315–352.

Endler JA, **Westcott DA**, **Madden JR**, **Robson T. 2005.** Animal visual systems and the evolution of color patterns: sensory processing illuminates signal evolution. *Evolution* **59:** 1795–1818.

Evanno G, **Regnaut S**, **Goudet J. 2005.** Detecting the number of clusters of individuals using the software STRUCTURE: a simulation study. *Molecular Ecology* **14:** 2611–2620.

Excoffier L, **Smouse PE**, **Quattro JM. 1992.** Analysis of molecular variance inferred from metric distances among DNA haplotypes: application to human mitochondrial DNA restriction data. *Genetics* **131:** 479–491.

Fuchs J, **Pons JM**, **Liu L**, **Ericson PGP**, **Couloux A**, **Pasquet E. 2013.** A multi-locus phylogeny suggests an ancient hybridization event between *Campephilus* and melanerpine woodpeckers (Ayes: Picidae). *Molecular Phylogenetics and Evolution* **67:** 578–588.

Gay L, **Neubauer G**, **Zagalska-Neubauer M**, **Pons JM**, **Bell DA**, **Crochet PA. 2009.** Speciation with gene flow in the large white-headed gulls: does selection counterbalance introgression? *Heredity* **102:** 133–146.

Gee JM. 2003. How a hybrid zone is maintained: behavioral mechanisms of interbreeding between California and Gambel's Quail (*Callipepla californica* and *C. gambelii*). *Evolution* **57:** 2407–2415.

Grant BR, **Grant PR. 2010.** Songs of Darwin's finches diverge when a new species enters the community. *Proceedings of the National Academy of Sciences of the United States of America* **107:** 20156–20163.

Grether GF, **Anderson CN**, **Drury JP**, **Kirschel ANG**, **Losin N**, **Okamoto K**, **Peiman KS. 2013.** The evolutionary consequences of interspecific aggression. *Annals of the New York Academy of Sciences* **1289:** 48–68.

Grether GF, **Peiman KS**, **Tobias JA**, **Robinson BW. 2017.** Causes and consequences of behavioral interference between species. *Trends in Ecology & Evolution* **32:** 760–772.

Haldane JBS. 1922. Sex ratio and unisexual sterility in hybrid animals. *Journal of Genetics* **12:** 101–109.

Harshman J. 1994. Reweaving the tapestry: what can we learn from Sibley and Ahlquist (1990). *The Auk* **111:** 377–388.

Hart NS, **Partridge JC**, **Cuthill IC**, **Bennett ATD. 2000.** Visual pigments, oil droplets, ocular media and cone photoreceptor distribution in two species of passerine bird: the blue tit (*Parus caeruleus* L.) and the blackbird (*Turdus merula* L.). *Journal of Comparative Physiology A* **186:** 375–387.

Hatfield T, **Schluter D. 1999.** Ecological speciation in sticklebacks: environment-dependent hybrid fitness. *Evolution* **53:** 866–873.

Jakobsson M, **Rosenberg NA. 2007.** CLUMPP: a cluster matching and permutation program for dealing with label switching and multimodality in analysis of population structure. *Bioinformatics* **23:** 1801–1806.

Johnsgard PA. 1967. Sympatry changes and hybridization incidence in Mallards and Black Ducks. *American Midland Naturalist* **77:** 51–63.

Johnson NK, **Johnson CB. 1985.** Speciation in Sapsuckers (*Sphyrapicus*): II. Sympatry, hybridization, and mate preference in *S. ruber daggetti* and *S. nuchalis*. *The Auk* **102:** 1–15.

Jombart T. 2008. *adegenet*: a R package for the multivariate analysis of genetic markers. *Bioinformatics* **24:** 1403–1405.

Jombart T, **Devillard S**, **Balloux F. 2010.** Discriminant analysis of principal components: a new method for the analysis of genetically structured populations. *BMC Genetics* **11:** 94.

Joseph L, **Dolman G**, **Donnellan S**, **Saint KM**, **Berg ML**, **Bennett ATD. 2008.** Where and when does a ring start and end? Testing the ring-species hypothesis in a species complex of Australian parrots. *Proceedings of the Royal Society B: Biological Sciences* **275:** 2431–2440.

Kamvar ZN, **Tabima JF**, **Grünwald NJ. 2014.** *Poppr*: an R package for genetic analysis of populations with clonal, partially clonal, and/or sexual reproduction. *PeerJ* **2:** e281.

Kearse M, **Moir R**, **Wilson A**, **Stones-Havas S**, **Cheung M**, **Sturrock S**, **Buxton S**, **Cooper A**, **Markowitz S**, **Duran C**, **Thierer T**, **Ashton B**, **Meintjes P**, **Drummond A. 2012.** Geneious Basic: an integrated and extendable desktop software platform for the organization and analysis of sequence data. *Bioinformatics* **28:** 1647–1649.

Kirkpatrick M, **Barton NH. 1997.** Evolution of a species' range. *The American Naturalist* **150:** 1–23.

Kirschel ANG, **Blumstein DT**, **Cohen RE**, **Buermann W**, **Smith TB**, **Slabbekoorn H. 2009a.** Birdsong tuned to the environment: green hylia song varies with elevation, tree cover, and noise. *Behavioral Ecology* **20:** 1089–1095.

Kirschel ANG, **Blumstein DT**, **Smith TB. 2009b.** Character displacement of song and morphology in African tinkerbirds. *Proceedings of the National Academy of Sciences of the United States of America* **106:** 8256–8261.

Kirschel ANG, **Nwankwo EC**, **Gonzalez JCT. 2018.** Investigation of the status of the enigmatic White-chested Tinkerbird *Pogoniulus makawai* using molecular analysis of the type specimen. *Ibis* **160:** 673–680.

Kirschel ANG, **Slabbekoorn H**, **Blumstein DT**, **Cohen RE**, **de Kort SR**, **Buermann W**, **Smith TB. 2011.** Testing alternative hypotheses for evolutionary diversification in an african songbird: rainforest refugia versus ecological gradients. *Evolution* **65:** 3162–3174.

Klein A, **Horsburgh GJ**, **Kupper C**, **Major A**, **Lee PL**, **Hoffmann G**, **Matics R**, **Dawson DA. 2009.** Microsatellite markers characterized in the barn owl (*Tyto alba*) and of high utility in other owls (Strigiformes: AVES). *Molecular Ecology Resources* **9:** 1512–1519.

Klicka J, **Fry AJ**, **Zink RM**, **Thompson CW. 2001.** A cytochrome-*b* perspective on *Passerina* bunting relationships. *The Auk* **118:** 611–623.

Kocher TD, **Thomas WK**, **Meyer A**, **Edwards SV**, **Pääbo S**, **Villablanca FX**, **Wilson AC. 1989.** Dynamics of mitochondrial-DNA evolution in animals: amplification and sequencing with conserved primers. *Proceedings of the National Academy of Sciences of the United States of America* **86:** 6196–6200.

Kumar S, **Stecher G**, **Tamura K. 2016.** MEGA7: molecular evolutionary genetics analysis version 7.0 for bigger datasets. *Molecular Biology and Evolution* **33:** 1870–1874.

Laiolo P. 2012. Interspecific interactions drive cultural co-evolution and acoustic convergence in syntopic species. *Journal of Animal Ecology* **81:** 594–604.

Lanfear R, **Frandsen PB**, **Wright AM**, **Senfeld T**, **Calcott B. 2016.** PartitionFinder 2: new methods for selecting partitioned models of evolution for molecular and morphological phylogenetic analyses. *Molecular Biology and Evolution* **34:** 772–773.

Lê S, **Josse J**, **Husson F. 2008.** FactoMineR: an R package for multivariate analysis. *Journal of Statistical Software* **25:** 1–18.

Leigh JW, **Bryant D**, **Nakagawa S. 2015.** POPART: full-feature software for haplotype network construction. *Methods in Ecology and Evolution* **6:** 1110–1116.

Lerner HRL, **Meyer M**, **James HF**, **Hofreiter M**, **Fleischer RC. 2011.** Multilocus resolution of phylogeny and timescale in the extant adaptive radiation of Hawaiian honeycreepers. *Current Biology* **21:** 1838–1844.

Littlejohn MJ, **Watson GF. 1985.** Hybrid zones and homogamy in Australian frogs. *Annual Review of Ecology and Systematics* **16:** 85–112.

Lovette IJ, **Bermingham E**, **Rohwer S**, **Wood C. 1999.** Mitochondrial restriction fragment length polymorphism (RFLP) and sequence variation among closely related avian species and the genetic characterization of hybrid *Dendroica* warblers. *Molecular Ecology* **8:** 1431–1441.

Maia R, **Eliason CM**, **Bitton PP**, **Doucet SM**, **Shawkey MD. 2013.** pavo: an R package for the analysis, visualization and organization of spectral data. *Methods in Ecology and Evolution* **4:** 906–913.

McCarthy EM. 2006. *Handbook of avian hybrids of the world*. Oxford: Oxford University Press.

McDevitt AD, **Edwards CJ**, **O'Toole P**, **O'Sullivan P**, **O'Reilly C**, **Carden RF. 2009.** Genetic structure of, and hybridisation between, red (*Cervus elaphus*) and sika (*Cervus nippon*) deer in Ireland. *Mammalian Biology* **74:** 263–273.

McEntee JP, **Peñalba JV**, **Werema C**, **Mulungu E**, **Mbilinyi M**, **Moyer D**, **Hansen L**, **Fjeldså J**, **Bowie RCK. 2016.** Social selection parapatry in Afrotropical sunbirds. *Evolution* **70:** 1307–1321.

McLean AJ, **Toon A**, **Schmidt DJ**, **Hughes JM**, **Joseph L. 2017.** Phylogeography and geno-phenotypic discordance in a widespread Australian bird, the Variegated Fairy-wren, *Malurus lamberti* (Aves: Maluridae). *Biological Journal of the Linnean Society* **121:** 655–669.

Meirmans PG, **Hedrick PW. 2011.** Assessing population structure: F_{ST} and related measures. *Molecular Ecology Resources* **11:** 5–18.

Meise W. 1928. The spread of the carrion crow (Formenkreis *Corvus corone* L.) *Journal of Ornithology*. 76: 1–203.

Michalczuk J, **McDevitt AD**, **Mazgajski TD**, **Figarski T**, **Ilieva M**, **Bujoczek M**, **Malczyk P**, **Kajtoch L. 2014.** Tests of multiple molecular markers for the identification of Great Spotted and Syrian Woodpeckers and their hybrids. *Journal of Ornithology* **155:** 591–600.

Monadjem A, **Passmore NI**, **Kemp AC. 1994.** Territorial calls of allopatric and sympatric populations of 2 species of pogoniulus tinkerbarbet in Southern Africa. *Ostrich* **65:** 339–341.

Moore WS. 1995. Inferring phylogenies from mtDNA variation: mitochondrial-gene trees versus nuclear-gene trees. *Evolution* **49:** 718–726.

Nei M. 1978. Estimation of average heterozygosity and genetic distance from a small number of individuals. *Genetics* **89:** 583–590.

Nwankwo EC, **Pallari CT**, **Hadjioannou L**, **Ioannou A**, **Mulwa RK**, **Kirschel ANG. 2018.** Rapid song divergence leads to discordance between genetic distance and phenotypic characters important in reproductive isolation. *Ecology and Evolution* **8:** 716–731.

Oatley G, **De Swardt DH**, **Nuttall RJ**, **Crowe TM**, **Bowie RCK. 2017.** Phenotypic and genotypic variation across a stable white-eye (*Zosterops* sp.) hybrid zone in central South Africa. *Biological Journal of the Linnean Society* **121:** 670–684.

Orians GH, **Willson MF. 1964.** Interspecific territories of birds. *Ecology* **45:** 736–745.

Pfennig KS, **Allenby A**, **Martin RA**, **Monroy A**, **Jones CD. 2012.** A suite of molecular markers for identifying species, detecting introgression and describing population structure in spadefoot toads (*Spea* spp.). *Molecular Ecology Resources* **12:** 909–917.

Pielou EC. 1975. *Ecological diversity*. London: Wiley-Interscience.

Poelstra JW, **Vijay N**, **Bossu CM**, **Lantz H**, **Ryll B**, **Müller I**, **Baglione V**, **Unneberg P**, **Wikelski M**, **Grabherr MG**, **Wolf JBW. 2014.** The genomic landscape underlying phenotypic integrity in the face of gene flow in crows. *Science* **344:** 1410–1414.

Prevosti A, **Ocaña J**, **Alonso G. 1975.** Distances between populations of *Drosophila subobscura*, based on chromosome arrangement frequencies. *Theoretical and Applied Genetics* **45:** 231–241.

Price TD, **Kirkpatrick M. 2009.** Evolutionarily stable range limits set by interspecific competition. *Proceedings of the Royal Society B: Biological Sciences* **276:** 1429–1434.

Pritchard JK, **Stephens M**, **Donnelly P. 2000.** Inference of population structure using multilocus genotype data. *Genetics* **155:** 945–959.

Prlic A, **Bouckaert R**, **Heled J**, **Kühnert D**, **Vaughan T**, **Wu C-H**, **Xie D**, **Suchard MA**, **Rambaut A**, **Drummond AJ. 2014.** BEAST 2: a software platform for Bayesian evolutionary analysis. *PLoS Computational Biology* **10:** e1003537.

Pryke SR, **Griffith SC. 2006.** Red dominates black: agonistic signalling among head morphs in the colour polymorphic Gouldian finch. *Proceedings of the Royal Society B: Biological Sciences* **273:** 949–957.

Qvarnstrom A, **Haavie J**, **Saether SA**, **Eriksson D**, **Part T. 2006.** Song similarity predicts hybridization in flycatchers. *Journal of Evolutionary Biology* **19:** 1202–1209.

R Core Team. 2017. R: A language and environment for statistical computing. Available from https://www.R-project.org/

Rambaut A, **Drummond AJ. 2014.** TreeAnnotator version 2, Available from http://beast.community/treeannotator

Rambaut A, **Suchar MA**, **Xie D**, **Drummond AJ. 2014.** Tracer v1.6, Available from http://beast.bio.ed.ac.uk/Tracer

Randler C. 2002. Avian hybridization, mixed pairing and female choice. *Animal Behaviour* **63:** 103–119.

Rohwer S, **Bermingham E**, **Wood C. 2001.** Plumage and mitochondrial DNA haplotype variation across a moving hybrid zone. *Evolution* **55:** 405–422.

Ronquist F, **Teslenko M**, **van der Mark P**, **Ayres DL**, **Darling A**, **Höhna S**, **Larget B**, **Liu L**, **Suchard MA**, **Huelsenbeck JP. 2012.** MrBayes 3.2: efficient Bayesian phylogenetic inference and model choice across a large model space. *Systematic Biology* **61:** 539–542.

Rosenberg NA. 2004. DISTRUCT: a program for the graphical display of population structure. *Molecular Ecology Notes* **4:** 137–138.

Ross GJB. 1970. The specific status and distribution of *Pogoniulus pusillus* (Dumont) and *Pogoniulus chrysoconus* (Temminck) in Southern Africa. *Ostrich* **41:** 200–204.

Senn HV, **Swanson GM**, **Goodman SJ**, **Barton NH**, **Pemberton JM. 2010.** Phenotypic correlates of hybridisation between red and sika deer (genus *Cervus*). *Journal of Animal Ecology* **79:** 414–425.

Shannon CE. 1948. A mathematical theory of communication. *Bell System Technical Journal* **27:** 379–423.

Short LL. 1965. *Hybridization in the flickers (Colaptes) of North America*. New York: American Museum of Natural History.

Short LL, **Horne JFM. 2001.** *Toucans, barbets and honeyguides: Ramphastidae, Capitonidae and Indicatoridae*. Oxford: Oxford University Press.

Simpson EH. 1949. Measurement of diversity. *Nature* **163:** 688–688.

Slabbekoorn H, **Smith TB. 2002.** Habitat-dependent song divergence in the little greenbul: an analysis of environmental selection pressures on acoustic signals. *Evolution* **56:** 1849–1858.

Smith TB, **Harrigan RJ**, **Kirschel ANG**, **Buermann W**, **Saatchi S**, **Blumstein DT**, **de Kort SR**, **Slabbekoorn H. 2013.** Predicting bird song from space. *Evolutionary Applications* **6:** 865–874.

Stamatakis A. 2014. RAxML version 8: a tool for phylogenetic analysis and post-analysis of large phylogenies. *Bioinformatics* **30:** 1312–1313.

Stoddard MC, **Prum RO. 2008.** Evolution of avian plumage color in a tetrahedral color space: a phylogenetic analysis of New World buntings. *The American Naturalist* **171:** 755–776.

Stoddart JA, **Taylor JF. 1988.** Genotypic diversity: estimation and prediction in samples. *Genetics* **118:** 705–711.

Svedin N, **Wiley C**, **Veen T**, **Gustafsson L**, **Qvarnstrom A. 2008.** Natural and sexual selection against hybrid flycatchers. *Proceedings of the Royal Society B: Biological Sciences* **275:** 735–744.

Tajima F. 1989. Statistical method for testing the neutral mutation hypothesis by DNA polymorphism. *Genetics* **123:** 585–595.

Tegelström H, **Gelter HP. 1990.** Haldane's rule and sex biassed gene flow between two hybridizing flycatcher species (*Ficedula albicollis* and *F. hypoleuca*, Aves: Muscicapidae). *Evolution* **44:** 2012–2021.

Tobias JA, **Seddon N. 2009.** Signal design and perception in *Hypocnemis* antbirds: evidence for convergent evolution via social selection. *Evolution* **63:** 3168–3189.

Toews DPL, **Taylor SA**, **Vallender R**, **Brelsford A**, **Butcher BG**, **Messer PW**, **Lovette IJ. 2016.** Plumage genes and little else distinguish the genomes of hybridizing warblers. *Current Biology* **26:** 2313–2318.

Väli Ü, **Dombrovski V**, **Treinys R**, **Bergmanis U**, **Daróczi SJ**, **Dravecky M**, **Ivanovski V**, **Lontkowski J**, **Maciorowski G**, **Meyburg BU**, **Mizera T**, **Zeitz R**, **Ellegren H. 2010.** Widespread hybridization between the Greater Spotted Eagle *Aquila clanga* and the Lesser Spotted Eagle *Aquila pomarina* (Aves: Accipitriformes) in Europe. *Biological Journal of the Linnean Society* **100:** 725–736.

Vorobyev M, **Osorio D**, **Bennett ATD**, **Marshall NJ**, **Cuthill IC. 1998.** Tetrachromacy, oil droplets and bird plumage colours. *Journal of Comparative Physiology A* **183:** 621–633.

Wallace AR. 1876. *The geographic distribution of animals*. London: MacMillan.

Weir JT, **Faccio MS**, **Pulido-Santacruz P**, **Barrera-Guzmán AO**, **Aleixo A. 2015.** Hybridization in headwater regions, and the role of rivers as drivers of speciation in Amazonian birds. *Evolution* **69:** 1823–1834.

Weir JT, **Price TD. 2011.** Limits to speciation inferred from times to secondary sympatry and ages of hybridizing species along a latitudinal gradient. *The American Naturalist* **177:** 462–469.

Wiebe KL. 2000. Assortative mating by color in a population of hybrid northern flickers. *The Auk* **117:** 525–529.

Wilson AC, **Cann RL**, **Carr SM**, **George M**, **Gyllensten UB**, **Helm-Bychowski KM**, **Higuchi RG**, **Palumbi SR**, **Prager EM**, **Sage RD**, **Stoneking M. 1985.** Mitochondrial-DNA and two perspectives on evolutionary genetics. *Biological Journal of the Linnean Society* **26:** 375–400.

Supporting Material

Figure S1. Chromatic distance within and among populations of each phenotype in sympatry and allopatry. Comparisons are between allopatric *Pogoniulus pusillus pusillus* (RFT), sympatric *P. p. pusillus* (SRFT), allopatric *Pogoniulus chrysoconus extoni* (YFT) and sympatric *P. c. extoni* (SYFT).

Figure S2. Segment classification plot for allopatric and sympatric populations. Allopatric *Pogoniulus pusillus pusillus* (RFT) are shown in red, sympatric *P. p. pusillus* (SRFT) in blue, allopatric *Pogoniulus chrysoconus extoni* (YFT) in yellow and sympatric *P. c. extoni* (SYFT) in green.

Figure S3. A, B, tetracolourspace plot at the individual level (A) and the population mean (B). C, D, hue projection plot encapsulated within a sphere at the individual level (C) and population mean (D).

Figure S4. A, genotype accumulation curve based on a permutational test on the optimal number of markers required to distinguish sufficiently between individuals in the populations plateaued at six loci. B, estimates of global indices for population differentiation based on microsatellite data. Heterozygosity with population structure (H_{ST} and G_{ST}) was lower than heterozygosity without population structure (H_T and $G_{prime-ST}$). The extent of population differentiation (D), ranging from zero for a panmictic population to one for complete differentiation, revealed high differentiation at two loci (CAM13 and TG13009; Supporting Information, Table S7).

Figure S5. Discriminant principal components analysis illustrating genetic differentiation among samples from *Pogoniulus pusillus pusillus* allopatric, *Pogoniulus chrysoconus extoni* allopatric, and sympatric samples based on microsatellite data.

Figure S6. Dendrogram on the genetic distance of the populations using the microsatellite data. Allopatric *Pogoniulus pusillus pusillus* are more closely related to the sympatric *Pogoniulus chrysoconus extoni* / *P. p. pusillus* population from Tshaneni and an allopatric *P. c. extoni* population at Mahushe Shongwe. Allopatric *P. c. extoni* are more closely related to the sympatric *P. c. extoni* / *P. p. pusillus* populations from Mawewe and Mpofu.

Figure S7. Maximum likelihood phylogenetic tree (RAxML best tree) based on 1033 bp of cytochrome *b*. Individuals are labelled based on their phenotype such that those highlighted in red are phenotypically red-fronted tinkerbirds and those highlighted in yellow are phenotypically yellow-fronted tinkerbirds. There are eight individuals with red forecrowns and *Pogoniulus chrysoconus extoni* haplotypes, but only one individual with a yellow forecrown and a *Pogoniulus pusillus pusillus* haplotype.

Table S1. Factor loadings on body size variables with varimax rotated principal component (PC)1 and PC2.

Table S2. Factor loadings on bill size variables with varimax rotated principal component (PC)1 and PC2.

Table S3. Generalized linear mixed effects model results for body size principal component (PC)1. Values for each variable are from the last model in which they were included based on the corrected Akaike information criterion score. The best supported model included only significant fixed effects.
Table S4. Generalized linear mixed effects model results for body size principal component (PC)2. Values for each variable are from the last model in which they were included based on the corrected Akaike information criterion score. The best supported model included only significant fixed effects.
Table S5. Generalized linear mixed effects model results for bill size principal component (PC)1. Values for each variable are from the last model in which they were included based on the corrected Akaike information criterion score. The best supported model included only significant fixed effects.
Table S6. Generalized linear mixed effects model results for bill size principal component (PC)2. Values for each variable are from the last model in which they were included based on the corrected Akaike information criterion score. The best supported model included only significant fixed effects.
Table S7. Differentiation indices per locus.
Table S8. Genotypic richness and abundance indices.
Table S9. Cline centres and widths and their two log-likelihood support limits for the phenotypic traits hue, chroma and brightness of forecrown patch, and wing length, in addition to STRUCTURE Q scores from microsatellite markers and the cytochrome *b* haplotype.
Table S10. Summary of samples used in this study and analyses conducted with the samples.